# EVLA Memo 230
# Polarimetry with the VLA's P-band

Rick Perley and Eric Greisen
National Radio Astronomy Observatory, Socorro, NM

May 31, 2024

**Abstract**

We continue our development of low-frequency polarimetry by investigating the accuracy of the ionospheric Faraday rotation corrections provided by the AIPS program TECOR. By observing polarized sources through dawn and dusk, we conclude these corrections successfully remove the IFRM with an accuracy of $\sim 0.1\mathrm{rad/m}^2$. Subsequent polarimetric imaging of the Moon reveals an unexpected, and unexplained residual rotation measure of $\sim -0.75\,\mathrm{rad/m}^2$. This residual is seen in all six of our observations, with values ranging from -0.6 to -0.9 $\mathrm{rad/m}^2$. A similar offset is seen in observations of DA240 and 3C345, when comparing to WSRT observations. Presuming this offset is unassociated with the sources in our observations, we have removed it by utilizing the values determined from the lunar observations, allowing the intrinsic source RMs and EVPAs for DA240, 3C303 and 3C345 to be determined.

## 1 Motivation

Polarimetry at low frequencies is difficult. Antenna sensitivities are low, the fractional polarizations for most sources are low, and there are very few useful known polarized calibration sources. To this list must be added the complicating effects of ionospheric Faraday rotation, which can rotate the observed plane of polarization by up to a full turn at a wavelength of 1 meter on timescales of hours to minutes.

Low-frequency polarimetry is important scientifically – observations of the polarization, and depolarization, of radio sources give information on the physical state of sources and the media through which the polarized emission propagates that is not available in any other way. This, combined with the recent rapid growth in new low-frequency arrays, makes it important to enable reliable measurements of source polarization at frequencies below 1 GHz.

The VLA has long had a low-frequency capability. The P-band and 4-band receivers were installed in the 1980s, but have not been extensively utilized for science. The likely major reasons for this are the unique high-frequency capabilities of the VLA dominating user interest, and the poor observational characteristics of the P-band system. The VLA antennas were not designed for low frequency capabilities, resulting in an ad-hoc low frequency design. The VLA's Cassegrain optics prevents receivers being located at the focus. As a consequence, the P-band feeds are nearly one wavelength out of focus, resulting in the low efficiency and poor sidelobe structures of the primary beam.

The VLA's polarimetric capabilities at its high frequency bands were well established early in the array's development. However, polarimetry was only recently enabled for the P-band system which, unique to the VLA, utlizes linear-polarized receivers. In a series of EVLA memos starting in 2019, (# 207, 210, 219, and 226) we have developed the AIPS software and methodology to enable accurate polarimetry with the P-band system. The focus of the early memos was on sorting out the various dipole orientation and phasing issues necessary for obtaining the correct polarization amplitudes. The complicated issue of establishing the correct electric vector position angles (EVPA), which requires accurate removal of the ionospheric Faraday rotation (IFRM), was deferred until last year.

In this memo, we describe our recent efforts in establishing an effective IFRM correction, and have used this to measure the low-frequency intrinsic polarization characteristics of three polarized sources visible in the northern hemisphere – DA240, 3C303, and 3C345. As a result of this effort, we have uncovered a mysterious offset in the RM of these sources, and the moon, whose origin is unknown.

## 2 The Observations

The data utilized in this memo are from six VLA P-band observations of the Moon and three known polarized sources. The goals were to utilize the known lunar polarimetric characteristics of the Moon to complete the implementation of calibration of linear systems in AIPS, judge the efficacy of ionospheric Faraday rotation corrections, and determine the properties of some low frequency polarized calibrators.

The observations were taken over a considerable period of time, as shown in Table 1. In this table, the seventh

Table 1: **Observing Log for Planetary Body Observations**

| 1 | 2 | 3 | 4 | 5 | 6 | 7 | 8 | 9 |
|---|---|---|---|---|---|---|---|---|
| Array | Date | Freq(MHz) | Conf. | Code | Target | PhsCal | UnpolarizedCal | PolarizedCal |
| VLA | 10Aug2017 | 288–448 | D | D1 | Moon | none | 3C147,3C295 | DA240,3C345 |
| VLA | 06Aug2017 | 288–448 | C | C1 | Moon | J1941–1524 | 3C295,3C48 | 3C345 |
| VLA | 30Dec2018 | 288–448 | C | C2 | Moon | J1229+0203 | 3C147,3C286,3C295 | DA240,3C303,3C345 |
| VLA | 13Dec2022 | 288–448 | C | C3 | Moon | J1021+2159 | 3C147,3C295 | DA240,3C303,3C345 |
| VLA | 04Nov2023 | 288–448 | D | D2 | Moon | none | 3C147 | DA240 |
| VLA | 20Jan2024 | 288–448 | D→C | DC | Moon | none | 3C48,3C147 | DA240 |

column gives the calibrator source adjacent to the target source, the eighth column lists the strong, known unpolarized source used to calibrate the gains and polarizations of the antennas. The ninth column gives the linearly polarized calibrators used to determine the cross-hand phase for the linear-basis data, and for which we will determine the absolute polarization properties.

Further details for the VLA P-band lunar observations are given in Table 2, showing the coordinates of the sun and the moon for each observation, the angular separation between them, the on-source integration time on the moon, and the local times for the observation start, lunar transit, stop, sunrise and sunset.

Table 2: **Specifics for VLA P-band Lunar Observations**

| 1 | 2 | | 3 | | 4 | 5 | 6 | 7 | 8 | 9 | 10 |
|---|---|---|---|---|---|---|---|---|---|---|---|
| Code | Sun | | Moon | | $Sep^n$ | IntTime | Start | Transit | End | Sunrise | Sunset |
| | RA | Dec | RA | Dec | deg | min | MST | | | | |
| D1 | 03 09 | 17 40 | 14 45 | -10 58 | 171 | 120 | 21:30 | 23:30 | 01:50 | 05:09 | 18:58 |
| C1 | 09 04 | 16 42 | 19 52 | -18 27 | 162 | 280 | 19:40 | 23:00 | 03:15 | 05:23 | 19:03 |
| C2 | 18 36 | -23 10 | 13 24 | -03 15 | 75 | 450 | 01:55 | 07:10 | 12:20 | 07:12 | 17:08 |
| C3 | 17 21 | -23 08 | 09 34 | 19 51 | 122 | 320 | 00:45 | 04:05 | 08:15 | 07:04 | 16:59 |
| D2 | 14 36 | -15 16 | 08 24 | 24 39 | 100 | 210 | 03:05 | 05:30 | 08:10 | 06:30 | 17:11 |
| DC | 20 10 | -20 04 | 04 17 | 25 06 | 124 | 220 | 15:40 | 20:30 | 23:37 | 07:11 | 17:25 |

## 3 Calibration and Imaging

The VLA P-band data were taken with linearly-polarized receivers. Given the considerable advantages of calibration with circular systems, we transformed the linear-based data to circular, using the procedures detailed in EVLA Memo#229.

As detailed in that memo, the linear-based visibility data need to be 'pre-calibrated' to correct for gain imbalances in time and frequency, and to remove the phase offsets between the 'H' and 'V' analog channels prior to conversion to a circular basis. These require using 'CALIB' and 'BPASS' on an unpolarized source to obtain the parallel-hand gains, and 'VHDIF' on a polarized source to remove the cross-hand phase. DA240 is strongly preferred for this operation, as its NE hotspot has the highest polarized flux density (over 400 mJy), and was used for all databases except for the C1 observation, for which we had to use the much more weakly polarized source 3C345.

After conversion to a circular basis, all data were calibrated utilizing all the calibrator sources, since their intrinsic polarizations are not needed for circular-based data, using well-known techniques. Because we are not yet certain that the cross-polarization solving program 'PCAL' correctly handles polarized sources when a large IFRM is present,

we ran this program using unpolarized sources for the low frequency bands. The IFRM was then estimated using TECOR, and the resulting L-R phase rotations recorded in the database gain tables.

In general, for circular-basis data, an observation of a polarized calibrator source with known EVPA is required to remove the R-L phase (which for the VLA is not independently measured), utilizing the program 'RLDIF'. In our previous high-frequency work, using the VLA's L, S, C, and X-band receivers, we used the known EVPA of the planetary bodies to determine those for the polarized target sources.

A considerable benefit of utilizing linear feeds is that the EVPA reference angle is set by the orientation of the reference antenna feeds. Conversion of such data to a circular basis – presuming the pre-calibration summarized above is done – will result in a database for which the R-L phase calibration is not necessary. Hence, in the following, the program 'RLDIF' has not been run.

To check the forementioned claim, our procedure was to image both the moon and the target polarized sources with our P-band data. The program 'MARSP' was used to determine any offset in the lunar EVPA from the known intrinsic radial orientation. Any non-zero offset should indicate errors in our calibration regimen – either due to an incorrect IFRM correction, or some other unknown effect. As will be described in later sections, we have indeed found a significant non-radial component in our lunar P-band imaging.

# 4 Ionospheric Corrections

The ionosphere typically contributes 1 to 2 rad/m$^2$ IFRM under quiet solar activity, but can contribute up to 6 rad/m$^2$ under active solar conditions. At 1 meter wavelength, these will cause typical rotations of 1 to 2 radians, and occasionally a full turn of rotation on timescales from hours to minutes. Effective low-frequency polarimetry must therefore accurately remove this induced rotation in order to determine the source polarimetric characteristics.

The AIPS calibration software package contains the program 'TECOR' which estimates the IFRM (Ionospheric Faraday Rotation Measure) for a given observation. It utilizes global ionospheric TEC data determined from the GPS satellite network, and includes a global magnetic field model. The TEC data are provided as integrated column densities, so no height profile is utilized. For the purposes of the calculation, the program assumes the electron content is in an infinitesimally thin layer at a height of 400 km, and utilizes a model magnetic field at that height to calculate the line-of-sight Faraday rotation. The calculated IFRMs for the six VLA P-band observations, for the moon and polarized calibrators, are shown in Fig 1.

Our first attempts at validating this simple model were made by our REU student Bailee Wolfe in the summer of 2023, the results of which are reported in EVLA Memo #219. She used archive L-band calibrator data taken on 3C286, 3C138, and other strongly polarized sources, and concluded that the TECOR estimates of the IFRM are accurate to 0.1 to 0.2 rad/m$^2$.

Because this work was done at a relatively high frequency, the accuracy of our result was relatively poor – a 1 rad/m$^2$ IFRM rotates the plane of polarization at 1.5 GHz by only 1.3 degrees. The P-band data utilized in this memo enables a more accurate estimate to be made. To illustrate this, we have utilized the polarized emission from DA240 and the Moon for the 'D2' observation. These data were taken through dawn, resulting in a significant increase in IFRM by about 2 radians/m$^2$ – a change of nearly 120 degrees at 1 meter wavelength. We use the same methods utilized by us in EVLA Memo#219, summarized next.

The relation between the observed EVPA, $\chi_{obs}$, and the source EVPA, $\chi_{src}$, due to Faraday rotation by a magnetized plasma along the propagation path can be written

$$\chi_{obs} = \chi_{src} + \lambda^2 \times \mathrm{IFRM} \tag{1}$$

where $\chi_{src}$ represents the intrinsic EVPA, including any Faraday rotations arising from the source environment and any unmodelled contribution above the height of the GPS satellites. We make the reasonable assumption that the source EVPA, $\chi_{src}$, does not change over the length of any one observation, while the IFRM does, due to changing ionospheric TEC and changing line-of-sight orientation. We have, via TECOR, an estimate of the IFRM. We suppose that this estimate is incorrect by a scale factor $K$, and an offset $L$. We can then write

$$\mathrm{IFRM}_{\mathrm{tecor}} = K \times \mathrm{IFRM}_{\mathrm{true}} + L \tag{2}$$

from which we find the observed EVPA given by

$$\chi_{obs} = \left(\chi_{src} - \frac{L\lambda^2}{K}\right) + \frac{\lambda^2}{K} \times \mathrm{IFRM}_{\mathrm{tecor}} \tag{3}$$

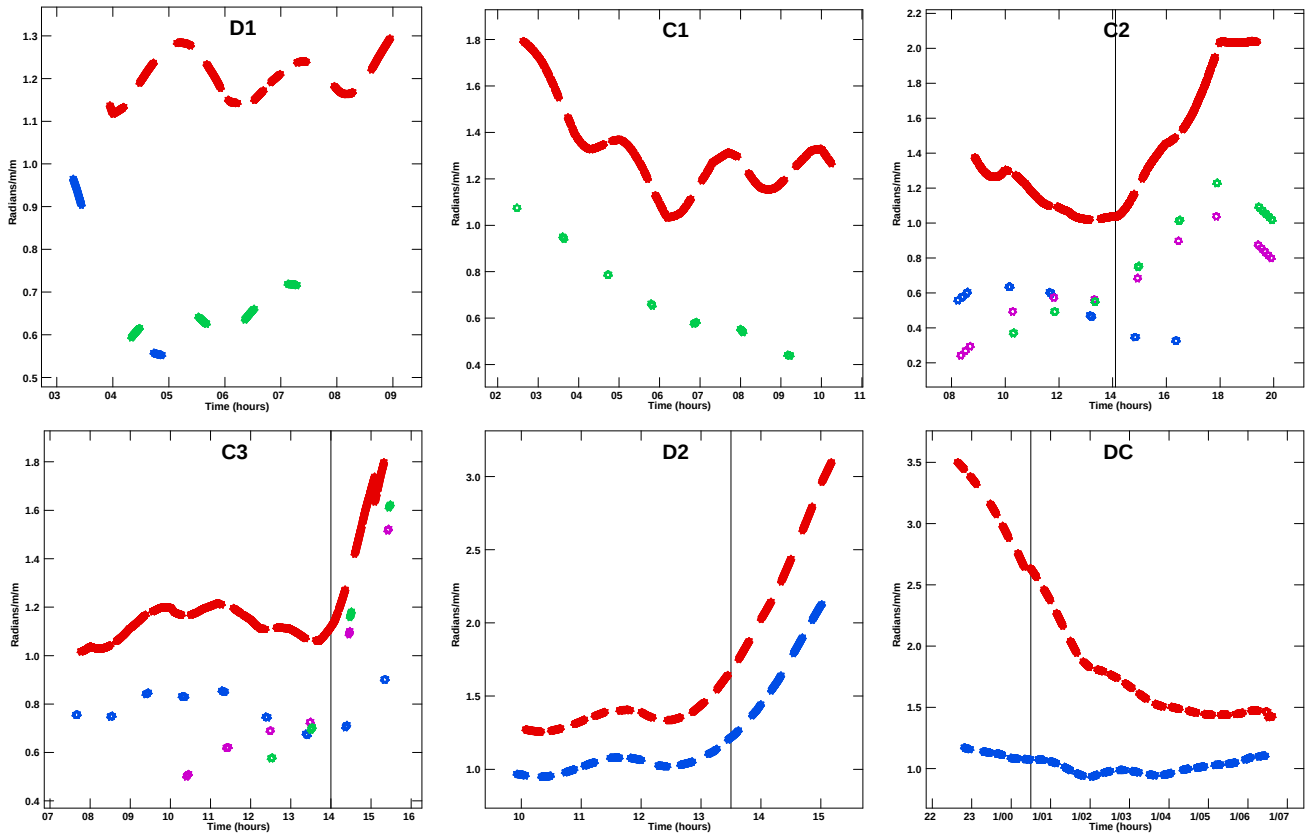


Figure 1: The TECOR estimates of the IFRM as a function of IAT time in hours for each of the six observations. Sources are color-coded: Moon in red, DA240 in blue, 3C303 in purple, and 3C345 in green. The thin vertical line in the C2, C3, and D2 panels indicate the time of sunrise, and sunset in the DC panel.

Plotting the observed $\chi_{obs}$ vs the estimated $\mathrm{IFRM}_{\mathrm{tecor}}$ for a given spectral window (frequency) should result in a linear slope given by $\lambda^2/K$ . A slope different than $\lambda^2$ is evidence of a scale error in the estimated IFRM. For example, if the estimated IFRM is too high by a factor of two, the resulting slope will be reduced by half – to $\lambda^2/2$. Random errors in the IFRM estimates will show up as horizontal deviations from the $\lambda^2$ linear dependence. The plot intercept is given by $\chi_{src} - L\lambda^2/K$. For the Moon, with a known intrinsic $\chi_{src} = 0$, the intercept should provide us any offset $L$ scaled by $-\lambda^2/K$.

We emphasize that this does not require knowledge of the source itrinsic polarization properties, nor the effects of any unmodeled RM above the height of the GPS satellites, as we are assuming these are constant in time over the length of the observation, and are analyzing data from the separate subands.

We show in Fig. 2 the results for DA240 and Moon, for the D2 observation. Each colored line represents the solution for a different spectral window. The legends in the two plots give the values of $\lambda^2$ and the measured slopes, for each spectral window. There is excellent agreement between these, indicating the estimated IFRMs are accurately tracking changes in the true values. The horizontal displacements between a plotted point and the best-fit line can be interpreted as the error in the IFRM. The maximum displacement seen is 0.1 rad/m$^2$ for the high SNR data from DA240, indicating the typical errors are less than this. The lunar data show a few greater offsets, but this is likely caused by the lower SNR of these observations.

The ratio of $\lambda^2$ to the measured slope provides an estimate of any scaling error in TECOR. Averaging all 16 observations of both the Moon and DA240 gives a ratio of $0.984 \pm 0.007$, thus marginal evidence that the IFRM is about 1.6% low. These results are in excellent agreement with our L-band work from last summer, and give us confidence that TECOR effectively removes the changing ionospheric rotation, at least for the stable conditions characteristic of these observations.

With the scale factor known to be close to $K = 1$, and with the known intrinsic EVPA of the moon being zero, the intercepts for each spectral window for the lunar data give us the negated offset scaled by $\lambda^2$. The formal solutions are shown in Table 3. The average scaled intercept, shown in the right-hand column, is $-0.821 \pm 0.025$ rad/m$^2$. For a

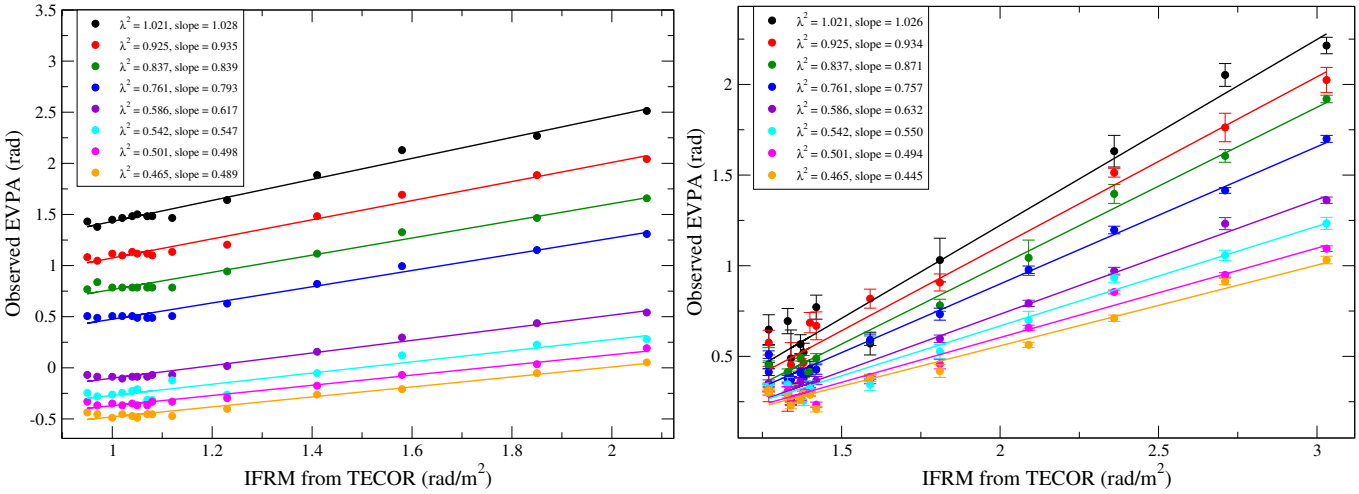


Figure 2: Plots of the observed EVPA vs the estimated IFRM for DA240 (left) and Moon (right). Each colored line represents the fit to a specific spectral window, identified in the legend with the appropriate wavelength squared. If the IFRM estimates from TECOR are correct, the slope of the linear fits should equal the wavelength squared. The results are shown in the legend. The horizontal offsets between the data and the fits suggest an accuracy of better than 0.1 rad/m$^2$, while the average of the ratio (slopes to $\lambda^2$) shows there is not a scaling error greater than 2% in the TECOR-based estimate of the IFRM.

Table 3: **EVPA Fits vs. estimated IFRM for the Moon**

| $\lambda^2$ | Slope | Slope/$\lambda^2$ | Intercept | Intercept/$\lambda^2$ |
|---|---|---|---|---|
| 1.021 | $1.026 \pm .063$ | 1.005 | $-0.828 \pm .113$ | -0.807 |
| 0.925 | $0.934 \pm .052$ | 1.010 | $-0.760 \pm .094$ | -0.822 |
| 0.837 | $0.871 \pm .032$ | 1.040 | $-0.738 \pm .059$ | -0.881 |
| 0.762 | $0.757 \pm .030$ | 0.993 | $-0.615 \pm .055$ | -0.807 |
| 0.586 | $0.632 \pm .024$ | 1.078 | $-0.531 \pm .044$ | -0.906 |
| 0.542 | $0.550 \pm .030$ | 1.015 | $-0.431 \pm .058$ | -0.795 |
| 0.501 | $0.494 \pm .023$ | 0.987 | $-0.383 \pm .042$ | -0.765 |
| 0.465 | $0.445 \pm .023$ | 0.957 | $-0.332 \pm .041$ | -0.714 |

general source, this would represent the source RM, plus that of any intervening unmodeled magnetized plasma. For the Moon, with a known intrinsic RM of zero, this offset in RM represents an additional source of RM not accounted for by the values provided by TECOR.

Another way to demonstrate the accuracy of the TECOR-based IFRM corrections is shown in Fig 3. Here, using the same data from the D2 observations, we plot the observed, and ionosphere-corrected, EVPA versus $\lambda^2$, at different times when the ionosphere is changing, using data taken through sunrise. Symbolically, we write

$$\chi_{obs} = \chi_{src} + (RM_{src} + IFRM)\lambda^2. \quad (4)$$

Presuming the IFRM is given by the value provided by TECOR, we define an adjusted value: $\chi_{adj} = \chi_{obs} - IFRM\lambda^2$, giving

$$\chi_{adj} = \chi_{src} + RM_{src}\lambda^2 \quad (5)$$

In the case of a linear fit versus the adjusted EVPA data, the measured slopes give the source intrinsic rotation measure for each time period, while the zero-intercept gives the intrinsic source EVPA[1]. The results of fitting the observed EVPA $\chi_{obs}$ and the adjusted (corrected for the IFRM) EVPA, $\chi_{adj}$ data are shown in Figure 3.

In this plot, the slope gives the observed RM, the intercept the intrinsic EVPA. For both sources, the fits to the uncorrected data are in the upper portions of the panels, the fits after correction by the IFRM values are shown

[1]Note that in this case, the resulting solutions are only meaningful if the source EVPA is not a function of wavelength. This presumes there is no internal or external depolarization (i.e., by 'beam' depolarization), and that the source polarization is not frequency-dependent. As will be seen in the next section, this presumption is well supported by the results from DA240, 3C345 and 3C303.

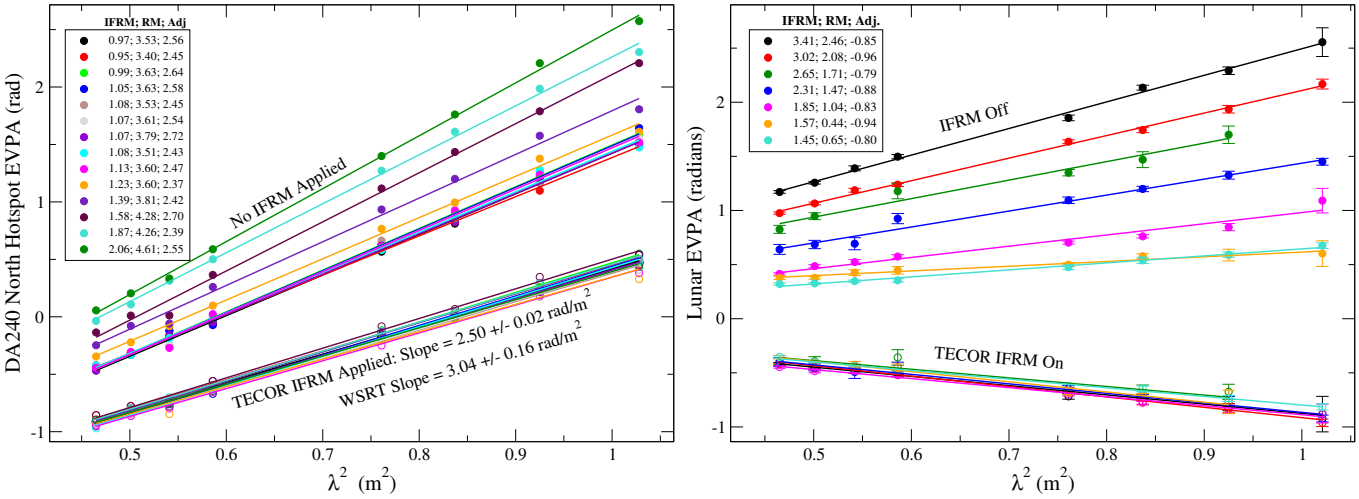


Figure 3: The observed, and IFRM-corrected, EVPAs for DA240 (left) and Moon (right), using the D2 dataset. For both, the data without the IFRM corrections are shown on top, and with the IFRM corrections applied on the bottom. For both sources, the corrections are very effective in removing the effects of the changing ionosphere. However, for both, the resulting relations show an apparent, negative residual RM, of $\sim -0.8$ rad/m$^2$. See the text for details.

below. The legend in each panel show the IFRM estimate, the measured slope to the uncorrected data, and the measured slope to the corrected data, all in rad/m$^2$.

It is immediately apparent in these plots that the IFRM corrections are very effective in removing the increasing rotation due to the thickening ionosphere. The left plot shows the observed and corrected EVPAs for the hotspot of DA240 for the 14 separate observations made that day. The first nine of these were taken before sunrise, and show no significant change in slope. Following dawn, very notable increases in the slope are observed, reflecting the additional rotation caused by the thickening ionosphere. Application of the estimated IFRM results in all data – before and after dawn – collapsing to a common relation, shown in the lower portion of the plot. The right panel shows the same information for the Moon on the same day. Note that the corrected EVPAs here do not have the expected slope of zero. That this residual acts like an unaccounted-for source of RM is evidenced by the perfectly linear relation with $\lambda^2$, and the zero EVPA offset intercept. These statements are shown more clearly in the left panel of Fig 4. Here, we show the uncorrected and corrected EVPA offsets from radial for the Moon, averaged for the times before sunrise. Shown in the legend are the slopes and intercepts. Note that the latter are zero, within the errors.

Two important points are shown in these figures:

1. The TECOR-estimated IFRMs are very effective in removing the changing EVPA caused by the changes in the ionosphere TEC and line-of-sight direction.

2. The source RMs and EVPAs, following the IFRM corrections, are not what are expected. For the Moon, the corrected EVPA deviations from radial must be zero at all frequencies – i.e., the corrected slopes should be zero, with zero intercepts. Yet we see a consistent residual, the same for all times, of about $-0.7$ rad/m$^2$. A similar, although smaller, discrepancy is seen in the values for DA240 – the expected value, measured with the WSRT is $3.04 \pm 0.16$, while we find $2.50 \pm 0.02$ rad/m$^2$.

This negative RM offset is seen in all six of our lunar observations, as shown in the right panel of Figure 4. This shows the small, but highly significant negative slopes in the IFRM-corrected data for all six lunar P-band observations. Note that the slopes are not all the same, suggesting that this residual contribution is variable. It is important to emphasize that, for all lunar observations, the zero-wavelength intercepts are always close to zero. These residual linear dependencies are indistinguishable from an additional, negative, component of RM, which is nearly constant for a given observation, and which is likely variable between observations.

The negative offsets are also seen in all observations of DA240 and 3C345, where we take the WSRT observation of Brentjens as the correct values. Using an intrinsic RM for the Moon of zero, $3.04 \pm 0.16$ rad/m$^2$ for DA240, and

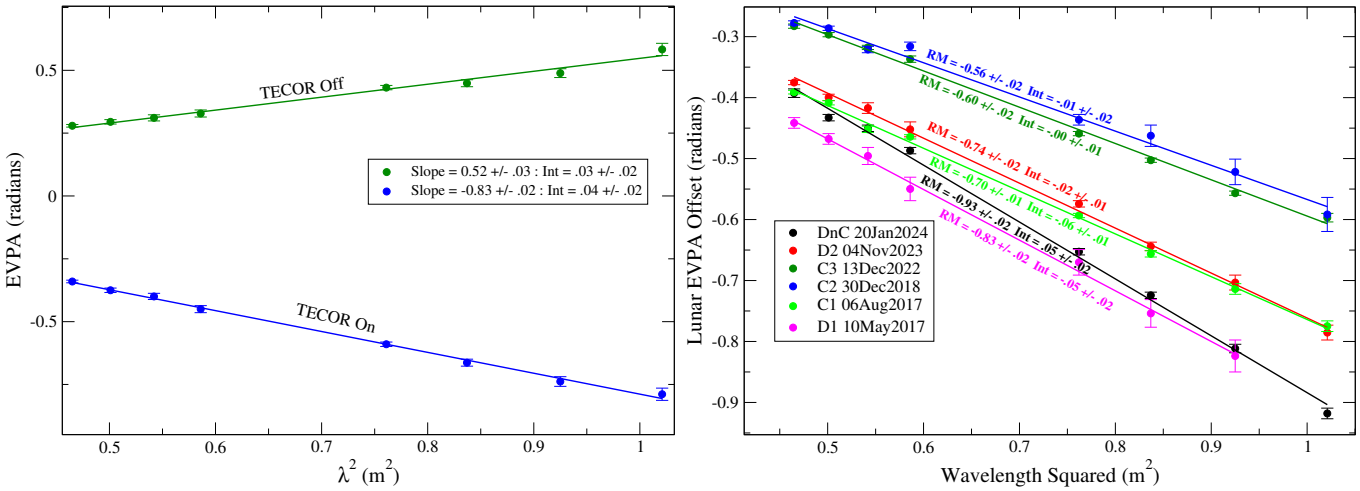


Figure 4: **Left Panel** Showing the lunar EVPA data without, and with, the IFRM correction. The data utilized are from the night-time portion of the D2 observation. Both fits have zero intercept, as expected (meaning the intrinsic fields are radial), but the corrected fit shows an 'excess' RM of -0.8 rad/m$^2$. This curious RM offset is seen in all our lunar datasets. **Right Panel** The residual lunar RM relations, after correction for the IFRM, for all six observations. There remains small, negative RM offsets whose origin is unkown.

Table 4: **RM Offsets for the Moon, DA240, and 3C345**

| Observation | Moon | DA240-North | 3C345 |
|---|---|---|---|
| D1 | $-0.74 \pm .02$ | $-0.28 \pm 0.2$ | $-1.65 \pm 0.6$ |
| C1 | $-0.70 \pm .02$ | - | $-1.30 \pm 0.6$ |
| C2 | $-0.60 \pm .02$ | $-0.42 \pm 0.2$ | $-1.22 \pm 0.6$ |
| C3 | $-0.56 \pm .02$ | $-0.46 \pm 0.2$ | $-1.53 \pm 0.6$ |
| D2 | $-0.74 \pm .02$ | $-0.58 \pm 0.2$ | - |
| DC | $-0.93 \pm .02$ | $-0.68 \pm 0.2$ | - |

$19.6 \pm 0.6$rad/m$^2$ for 3C345, the observed residual slopes for all six of our observations are shown in Table 4. The quoted errors for DA240 and 3C345 are dominated by the WSRT observations. Note that these errors are large enough that the apparent discrepancies between the two extragalactic sources and the moon are not statistically different. On the other hand, the differences for any given source between different observations is statistcally significant. Thus, except for the D1 observation of DA240, all offsets are consistent with a time-variant, and likely spatially invariant, RM offset. We are unsure of the reason for the slightly discrepant D1 result, but note that there were only two short observations of DA240 in that observation.

## 4.1 From Where Does this Residual Arise?

The obvious question is: What is the origin of these small, but highly significant RM residuals? We are confident they are not due to the AIPS software – they are seen exactly equally with both the original linear-basis data, and the converted circular-basis data. It cannot be due to an offset in the polarized lunar emission, as the zero-wavelength intercept is always zero, as expected. It is most unlikely to be due to a scaling error in the calculation of the IFRM – the scaling error would have to be by a factor of two or more, and we have shown in Figure 1 that any scaling error is very small. It is simply impossible for the TEC values, or magnetic field model to be in error by such a factor.

We have been unable to understand how the observing system, or the software, can introduce a rotation so precisely proportional to $\lambda^2$. We have asked others to utilize other reduction software packages to check our results, but have not received any confirmation to date. We have also tried to find some correlation between the various slopes shown in Fig 4 and variables such as time of day, lunar phase, lunar-solar offset, ionospheric IFRM, without success.

Can the excess RM arise from the earth's magnetosphere/plasmasphere, above the height of the GPS satellites? We can make a rough estimate of the required electron density and fields from the simple relation between rotation

measure and the electron density, path length, and magnetic fields. We have

$$RM \sim 0.8 n_e L B_{\|} \tag{6}$$

where $RM$ is the rotation measure in rad/m$^2$, $n_e$ is the electron density in cm$^{-3}$, $L$ is the path length in pc, and $B_{\|}$ is the line-of-sight magnetic field in microG. For the purposes of estimation, we set the length to the distance to the moon, $\sim 1.3 \times 10^{-08}$ pc, B in gauss, and $RM = 0.7$. From these, we find the excess RM of 0.7 rad/m$^2$ could be provided by a product of the mean electron density and magnetic field between here and the Moon given by:

$$n_e B_g \sim 70 \tag{7}$$

where the electron density is in cm$^{-3}$, and the line-of-sight magnetic field is in Gauss. An alternate relation, in terms of the electron column density, results in

$$RM \sim 3 \times 10^{-13} n_c B_G \tag{8}$$

where $n_c$ is the column density in cm$^{-2}$, and $B_G$ is the line-of-sight field in Gauss. According to Tracy Clarke (private communication) the column density above the plasmasphere is about 0.001 TECU = $10^9$cm$^{-2}$, requiring a magnetic field of at least 2 mG – far too high to account for our apparent residual.

Until such time that a viable explanation can be uncovered, we presume these offsets are constant over any one observing day, and apply equally to all sources observed on a given day. If it is eventually concluded these RM offsets are real, all the results quoted in the next section will need to be adjusted upwards by the value of the lunar RM slope on the day of observation.

# 5 Results for the Polarized Sources

Presuming TECOR is valid for all our observations, and that the observed residual lunar RMs apply equally to all sources observed on the day of observation, we have applied these offsets to the lunar and target source data. We show in the following section the results for each source.

## 5.1 DA240 West Hotspot

DA240 is a nearby radio galaxy with an unusually bright and highly polarized hotspot in its eastern lobe. An image with 46 arcseconds resolution at 424 MHz, using data from all five VLA P-band observations, showing the observed polarization, is shown in Fig 5. The source is very extended – spanning about 30 arcminutes. The prominent hotspot in the eastern lobe is easily seen, and is partially resolved. This hotspot is a very good low-frequency polarization calibrator for the VLA's C and D configurations as the polarized flux density exceeds 400 mJy.

The advantage of using radio galaxy or quasar hotspots for low-frequency polarimetry comes from their optically thin synchrotron emission – the fractional polarization and the intrinsic EVPA is the same over all frequencies, – and from their locations well outside the central cores of the associated galaxy. These offset locations should greatly reduce any differential ('beam') depolarization due to intervening galactic gas and reduce the total rotation measure.

The observed polarization EVPAs for DA240 are shown in Fig 5. The different observations are plotted with different colors, as shown in the figure legend. The data show a nearly perfect $\lambda^2$ relation, indicating that the slope represents the RM associated with the host galaxy and our own galaxy. There is no sign of non-linear behavior. The fractional polarization is $\sim 15$ to 20%, depending on resolution, with the higher fraction associated with higher resolution. Four of the five observations give very similar results, with a maximum spread of about ten degrees. The 'D1' observation has a notably steeper slope – these data were of poorer quality, and contain only two observations of the source. They were not used in the determination of the average (shown by the black points, and the black line). The remaining observations give very similar slopes, but with slightly different intercepts. We intepret this as the error associated with the determination of the IFRM – corresponding to 0.1 rad/m$^2$, the same error that we reported, using L-band data in our memo from last year.

The best-fit, global average RM is $3.17 \pm 0.02$ rad/m$^2$ – within 1-$\sigma$ of the WSRT value determined by Michiel Brentjens in his thesis. The determined intrinsic EVPA at $\lambda = 0$ is $-116 \pm 1$ degrees, which places the B-vector about orthogonal to the line joining the hotspot to the nucleus, as expected for structure of this type.

As noted, the hotspot is slightly resolved at this resolution. It is not yet known if the hotspot is useful as a polarization EVPA calibrator for the B and A configurations due to this resolution. We plan to make observations during the summer and fall of 2024 to make this determination.

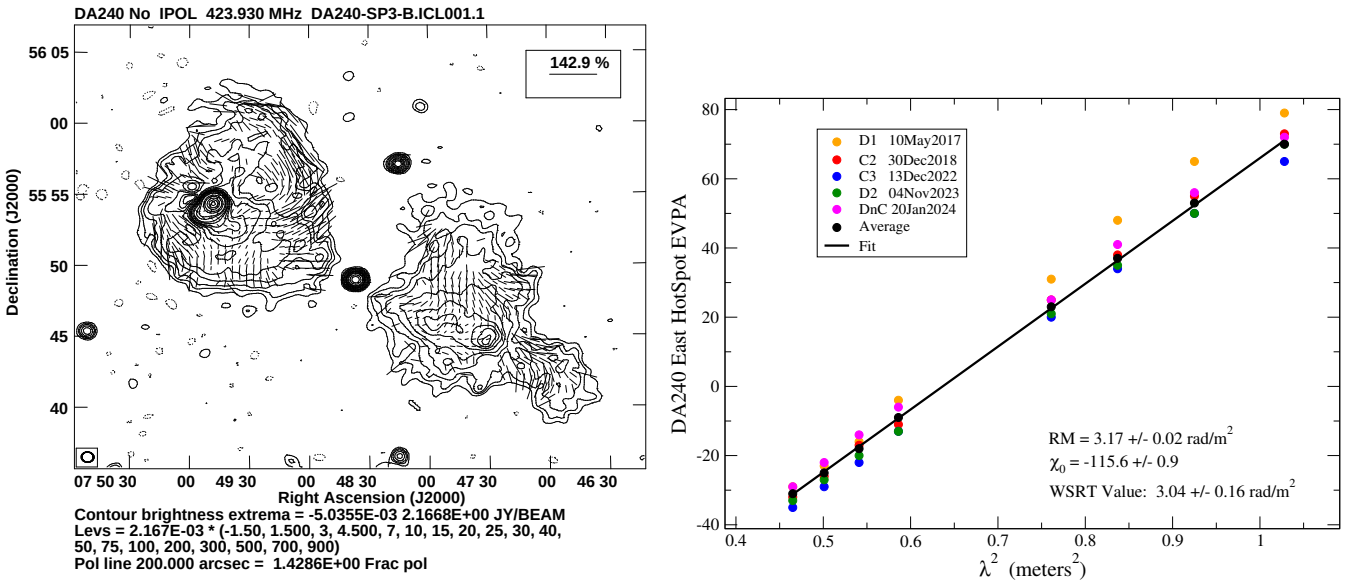


Figure 5: **Left Panel** The structure and polarization DA240 at 424 MHz with 46 arcseconds resolution, utilizing the data taken from all five observations. **Right Panel** The corrected EVPAs for the DA240 northern hotspot, for each of the five observations. The black points and fitted slope have excluded the D1 dataset.

## 5.2 3C303 West Hotspot

The Seyfert galaxy 3C303 has a very prominent, highly polarized hotspot, which makes it a prime candidate for a polarization calibrator. The source was observed on two dates. No image is shown here, as the 47 arcsecond extent is barely resolved to the VLA in C configuration. The determined EVPA, after correction for the IFRM, is shown in the left panel of Fig 6. The hotspot is 5.1% polarized (corresponding to ∼300 mJy polarized flux) at 424 MHz. The

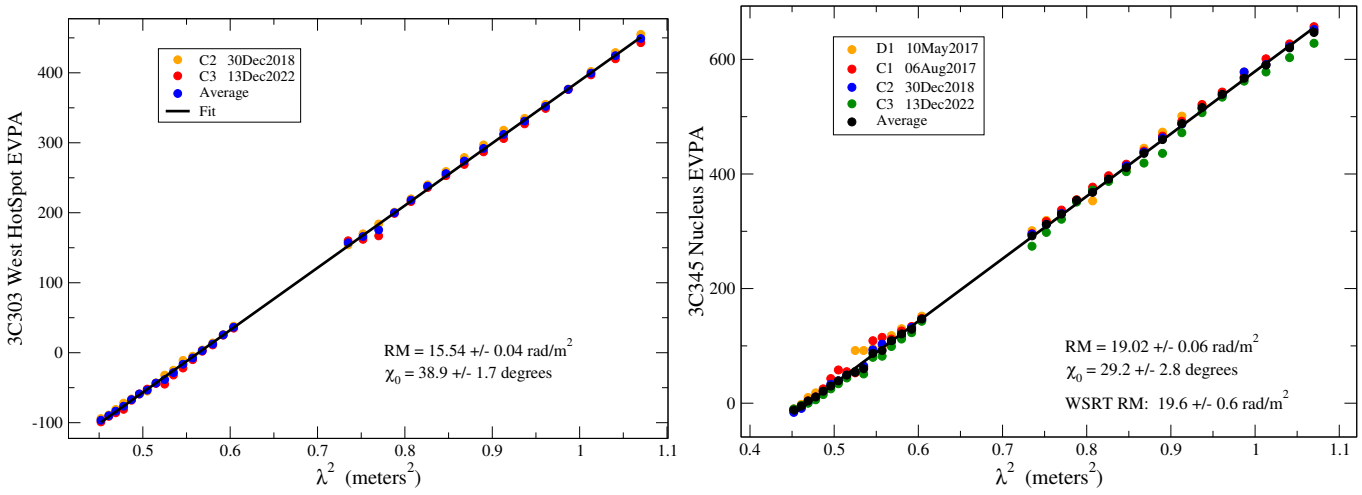


Figure 6: **Left** The fit of IFRM-corrected EVPA of 3C303 against $\lambda^2$. As with the other sources, a very clean linear fit is found. **Right** The fit for the IFRM-corrected EVPAs for 3C345.

excellent linear fit provides the source RM and intrinsic position angle solutions shown in the figure.

## 5.3 3C345 = J1642+3948

3C345 is a well known quasar, with a jet and bright hotspot extending to the NE some 3 arcseconds from the nucleus, embedded in a more extensive structure most prominent at low frequencies. It is only slightly resolved in

our 45-arcsecond resolution images. The polarized emission – likely from the hotspot – is only 3.3% of the total flux, making this source somewhat marginal as a polarization calibrator. It was observed four times in our program, and the resulting EVPAs are shown in Fig 6. The derived RM is $19.02 \pm 0.04$ rad/m$^2$, which is to be compared to the WSRT-determined value of 19.6$\pm$ 0.6 rad/m$^2$.

# 6 Summary

Our P-band polarimetric observations of the Moon, DA240, 3C345, and 3C303 have demonstrated that the IFRM corrections provided by the AIPS program TECOR are accurate to about 0.1 rad/m$^2$, or about 5 degrees at a wavelength of 1 meter, and are thus highly effective in removing the changing Faraday rotation due to the ionosphere. However, the resulting polarimetric images of the Moon, which is known to have an intrinsic RM of zero, and a radial orientation of the EVPA near the limb, show a small but highly signficant residual RM typically -0.6 to -0.9 rad/m$^2$. This residual is different on different days. We have not been able to find the origin of this residual – it is unlikely to have been caused by the calibration software or the telescope array, and is highly unlikely to originate in any scaling error in the IFRM corrections. A physical origin remains possible, but seems unlikely, given the known electron densities and magnetic fields between the height of the GPS satellites and the lunar surface.